Available online at www.sciencedirect.com
ScienceDirect
Trans. Nonferrous Met. Soc. China 33(2023) 2206−2215
Transactions of Nonferrous Metals Society of China
www.tnmsc.cn

# One-step electrolytic reduction desulfurization of $Sb_2S_3$ in different molten salts

Qiang ZHU, Jian-guang YANG, Chao-bo TANG, Rui-ze DING, Tian-xiang NAN, Qing-cheng HU

School of Metallurgy and Environment, Central South University, Changsha 410083, China

Received 2 March 2022; accepted 5 July 2022

**Abstract:** A comparative analysis of different molten salt systems was conducted, including NaCl−KCl, NaCl−$CaCl_2$, NaCl−$Na_2CO_3$, NaCl−KCl−$CaCl_2$, and NaCl−KCl−$Na_2CO_3$. The phase diagrams, thermal stability, and solubility of $Sb_2S_3$ in molten salt systems were investigated. Based on the distribution of the element antimony, current efficiency, energy consumption, and the characterization of the residue, the most suitable molten salt for the electrical reduction of $Sb_2S_3$ was verified. The results show that all molten salt systems have good thermal stability and can realize the electrolytic reduction of $Sb_2S_3$. The system with $CaCl_2$ is not conducive to the dissolution of $Sb_2S_3$, and the system with $Na_2CO_3$ can react with $Sb_2S_3$. In addition, the current efficiency of the NaCl−KCl system is the highest (75.68%), and the energy consumption ratio is the lowest (2.18 kW·h/kg).

**Key words:** antimony smelting; molten salt electrolysis; $Sb_2S_3$; eutectic system

## 1 Introduction

Stibnite ($Sb_2S_3$) is the primary raw material for antimony extraction [1]. Since the discovery of the volatile properties of antimony sulfide and antimony oxide, $Sb_2S_3$ oxidized to $Sb_2O_3$ and then reduced to metal antimony technology (oxidation volatile roasting−reduction smelting process), has become the primary method of antimony smelting used so far [2,3]. Unfortunately, the coke reduction process produces a large amount of greenhouse gas $CO_2$ and emits low concentration $SO_2$ flue gas that is not conducive to acid production. Long-term industrial production leads to the environmental pollution and extreme climate [4−7]. Theoretically, hydrometallurgical technology can effectively avoid the above problems. However, the alkali method is rarely used because of its low current efficiency and high energy consumption [8,9]. Antimony explosion is one major problem when the acid method is applied in the electrodeposition. The technology has not been used to produce metal antimony, but only in small-scale production of high purity antimony oxide [10,11].

In recent years, the electrolytic process of molten salt to prepare aluminum, titanium, and rare earth metal from oxides or alloys has witnessed many research achievements [12,13]. LU et al [14] proposed a solid-state electrolysis (SSE) process for upcycling aluminum from aluminum casting alloys. CHEN et al [15] proposed FFC (Fray−Farthing−Chen) electrolysis technology with molten $CaCl_2$ as the electrolyte to electrolyze solid $TiO_2$ to metal titanium successfully.

Due to the advantages of low power consumption, without carbon emission, and without $SO_2$ generation, molten salt electrolysis technology of sulfide also attracts more and more attention. It is worthwhile that sulfide has a low melting point and good electrical conductivity in the molten state. Direct electrolytic molten sulfide is challenging to

**Corresponding author:** Jian-guang YANG, Tel: +86-731-88830470, E-mail: jianguang_y@163.com
DOI: 10.1016/S1003-6326(23)66253-3

achieve sulfur separation [16−18]. Therefore, diluting sulfide with molten salt to avoid electron conduction of electrolytes is the key to effective electrolysis. TAN et al [19] found that $CuFeS_2$ had controllable solubility in molten NaCl−KCl, and ensured high ionic conductivity in the electrolysis process. Besides, YIN et al [20] explained the electrolysis process of $Sb_2S_3$ in a molten semiconductor. The migration rate of $S^{2-}$ was critical to affecting the current efficiency [20−22]. However, in the current NaCl−KCl system, there are some problems in the electrolytic process of $Sb_2S_3$, such as low current efficiency, high energy consumption, and considerable material loss. Therefore, we conducted a comparative study on different molten salt systems, to select a molten salt system that is beneficial to improving current efficiency and reducing energy consumption and raw material loss.

The phase diagrams of NaCl−KCl (NK), $CaCl_2$−NaCl (CN), $Na_2CO_3$−NaCl (NN), $CaCl_2$−NaCl−KCl (CNK), and $Na_2CO_3$−NaCl−KCl (NNK) were analyzed by FactSage software. At the mass ratio of the lowest eutectic temperature, the thermal stability (stability and volatility of components) and the solubility of antimony sulfide were investigated [23]. Moreover, the constant piezoelectric reduction desulfurization process of $Sb_2S_3$ was studied. This provides theoretical guidance for further saving energy and reducing raw material consumption in molten salt electrolysis of $Sb_2S_3$.

## 2 Experimental

### 2.1 Preparation of electrolyte

The molten salts used in the experiment were all analytical reagents, including NaCl, KCl, $CaCl_2$, $Na_2CO_3$, $Na_2S·9H_2O$, and $Sb_2S_3$. All molten salt components were mechanically mixed for 0.5 h. Then, it was dehydrated for 24 h in an inert atmosphere of 250 °C and heated to 900 °C to form liquid molten salt, and it was thoroughly mixed through the gas pipe for 1 h. Finally, the molten salt was cooled down, ground again, and preserved in a vacuum to be the raw material for the test.

### 2.2 Thermal stability and dissolution test

The molten salt thermal stability test was carried out in an inert atmosphere at 850 °C. After being cooled, its mass and phase were recorded. In the solubility test, 30 g of $Sb_2S_3$ and 100 g of prepared molten salt were successively filled into a corundum crucible with a diameter of 5 cm and a height of 15 cm, and they were held for 3 h in an inert atmosphere of 850 °C. The crucible was broken after cooling, and the phenomena were observed. The samples of the upper molten salt were ground into uniform powder and stored for analysis.

### 2.3 Constant-voltage electrolytic test

As shown in Fig. 1, the constant-voltage electrolysis process was carried out in a self-made vertical electrolytic cell composed of a graphite crucible (110 mm in inner diameter, 120 mm in outer diameter, and 150 mm in depth) and a corundum crucible with a hole of 5 cm in diameter at the bottom. $Sb_2S_3$ (100 g) and mixed molten salt (500 g) were successively transferred to a combined electrolytic cell with nitrogen (>99.999%) [20]. $Na_2S·9H_2O$ (30.8 g) was added to the molten salt surface, and the electrolytic furnace was opened according to the pre-set heating program. When the furnace temperature reached the set value, the electrolytic anode (acted by graphite block, 50 mm long, 50 mm wide, and 100 mm high) was placed in the molten salt on the upper layer and the pole spacing was adjusted to be 4 cm. A high-power DC power supply (IT6722A mode) could provide a stable 2.5 V constant voltage. The current of the electrolytic process was recorded, the switch of the DC power supply was turned off 3 h later, the anode was removed from the molten salt, and heating was stopped. When cooling was over, all dust, molten salt residue, and metallic crude antimony were

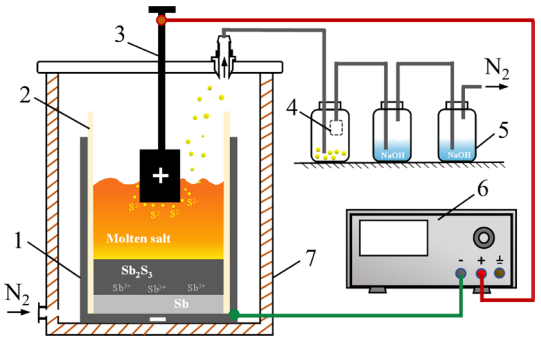


**Fig. 1** Schematic diagram of reaction device for antimony electrolysis in molten salts: 1−Graphite crucible; 2−Corundum casing; 3−Graphite anode; 4−Dust collector; 5−Washing bottle; 6−Direct-current power supply; 7−Hearth

collected. Meanwhile, it was ground into a uniform powder and sealed for analysis.

### 2.4 Sample characterization

All sample masses were recorded by analytical balance. Current data was recorded according to the real-time display on the DC power supply screen. The elemental content of crude antimony, molten salt, and dust was measured by ICP-AES (PerkinElmer, Optima 3000, QC, Norwalk, USA). Furthermore, SEM−EDS (Kabuskiki Kaisha, JSM−7900F, Japan; EDS, Oxford, INCA Wave 8570, UK) was used to observe the microstructure and elemental occurrence characteristics of molten salts after the dissolution and electro-decomposition of $Sb_2S_3$ in each system. XRD (PANalytical, Cu $K_\alpha$ radiation, $\lambda$=1.54 Å, Empyrean 2, Netherland) was used to analyze the phase characteristics of the residues from dissolution and electrolysis tests.

## 3 Results and discussion

### 3.1 Phase diagram analysis

As shown in Fig. 2, phase diagrams of molten salt systems were drawn by Fasage thermodynamic calculation software. The ratio of molten salt studied in each system was determined according to the lowest eutectic temperature of binary or ternary phase diagrams. The lowest eutectic temperatures of NK system, CN system and NN system were 656, 506 and 631.2 °C at the mass ratios of NaCl/(KCl+NaCl)=0.44, $CaCl_2$/($CaCl_2$+NaCl)=0.67 and $Na_2CO_3$/($Na_2CO_3$+NaCl)=0.59, respectively. The minimum eutectic temperatures of CN and NN systems were reduced by 50 and 24.8 °C compared with those of the NK system. Ternary CNK and CNN systems had lower eutectic temperatures than binary systems. The lowest eutectic temperatures of two systems were 483.1 and 552.5 °C, respectively. The corresponding ratio of molten salt was $CaCl_2$:NaCl:KCl=0.66:0.27:0.07, and $Na_2CO_3$:NaCl:KCl=0.33:0.28:0.39. Therefore, according to the results of theoretically calculated eutectic temperature, it can be seen that adding $CaCl_2$ or $Na_2CO_3$ can reduce the theoretical temperature of molten salt electrolysis. Moreover, the more complex the molten salt system is, the lower the temperature is required to form a molten state.

### 3.2 Thermal stability of molten salt

The thermal stability of molten salt is the key factor affecting the selection of a molten salt electrolysis system. Loss or change of molten salt components inevitably leads to high costs. Molten salt volatilization of different systems was measured at 850 °C for 5 h (Fig. 3(a)). The results show that the average volatilization per hour was 1.46% for NK, 0.96% for NNK, 0.66% for CN,

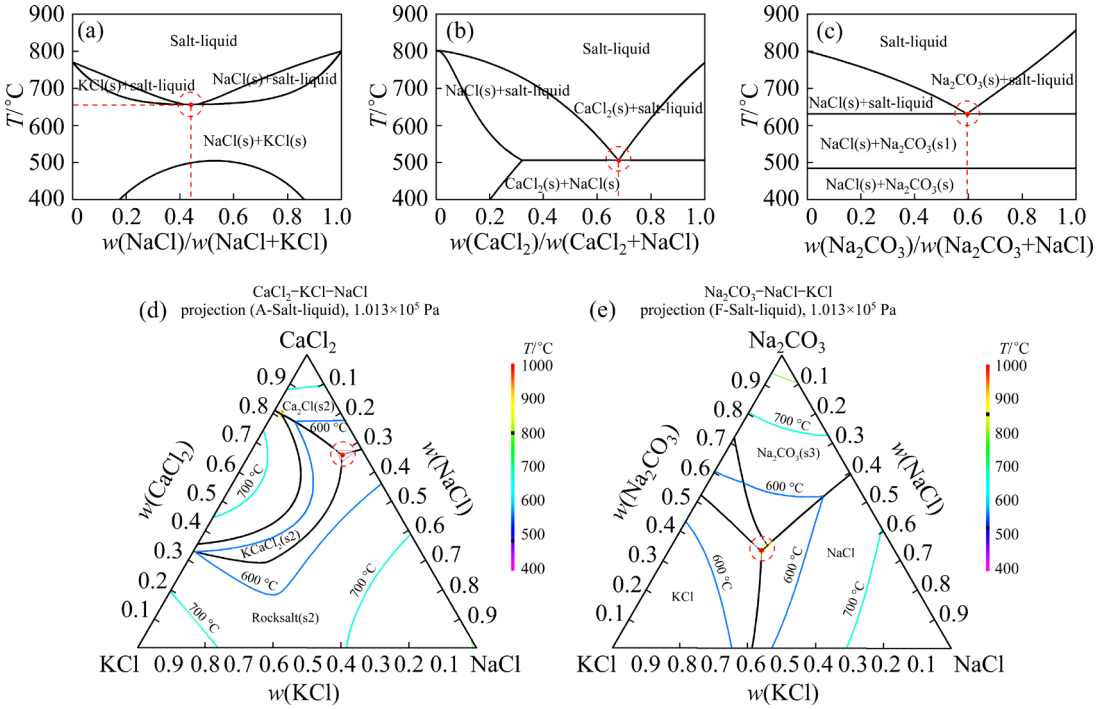


**Fig. 2** Phase diagrams of different molten salt systems: (a) NK; (b) CN; (c) NN; (d) CNK; (e) NNK

0.45% for CNK, and 0.20% for NN. In NK, NNK, and CNK systems, as the proportion of NaCl−KCl increased, the volatilization of molten salt in the whole system also increased. In the CN and CNK systems, $CaCl_2$ had a similar mass ratio, but the volatilization of the latter decreased obviously. These results indicate that eutectic NaCl−KCl may have better volatilization stability than NaCl alone in a molten state. The comparison with NK and NNK systems shows that adding $Na_2CO_3$ reduces the volatilization of the molten salt. Especially for the NN system, the volatilization of molten salt per hour is only 0.20%. As shown in Fig. 3(b), NK, NN, and NNK systems can maintain the original molten salt phase at 850 °C. In CN and CNK systems, the phase of $CaCl_2(H_2O)_2$ can also be found in addition to the original molten salt phase, mainly due to the excellent water absorption of $CaCl_2$ and water absorption during the detection process.

### 3.3 Dissolution characteristics of $Sb_2S_3$ in molten salt

The dissolution tests were conducted in an inert atmosphere to investigate the dissolution characteristics and rules of $Sb_2S_3$ in different systems. As seen in Fig. 4, $Sb_2S_3$ was dissolved in different molten salt systems, and the side view and elevation view of the dissolved phase were obtained after rapid cooling. In NK, NC, and CNK systems, it can be found that the dissolved phase can be divided into sulfide and molten salt with apparent stratification. This phenomenon indicates that the solubility of $Sb_2S_3$ is low. The density of molten NaCl, KCl, and $CaCl_2$ is less than that of sulfide. In NN and NNK systems, the whole molten salt was pale yellow, and no sulfide phase was found. This phenomenon shows that part of $Sb_2S_3$ reacts with $Na_2CO_3$ to precipitate metallic antimony, as shown in Reaction (1). The other part of $Sb_2S_3$ is dissolved

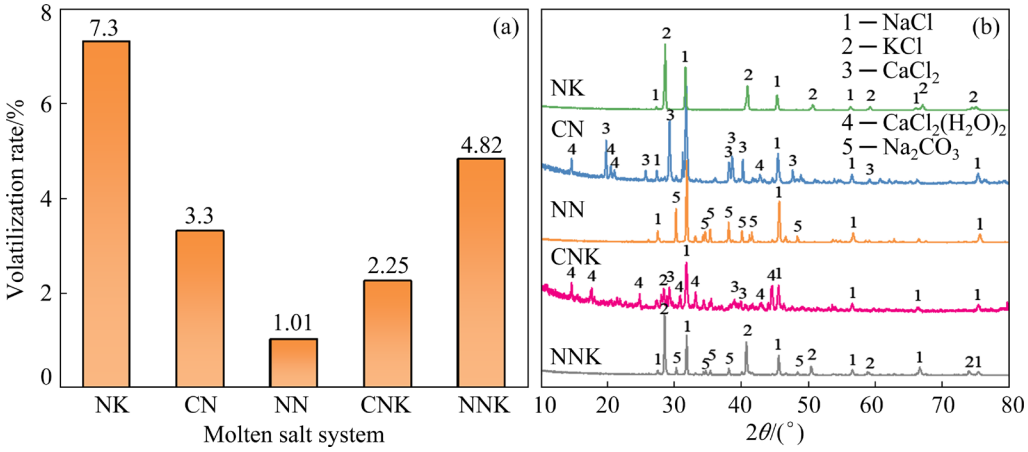


**Fig. 3** Stability of different molten salts held at 850 °C for 5 h: (a) Volatility of molten salts; (b) XRD patterns of molten salts after high-temperature holding

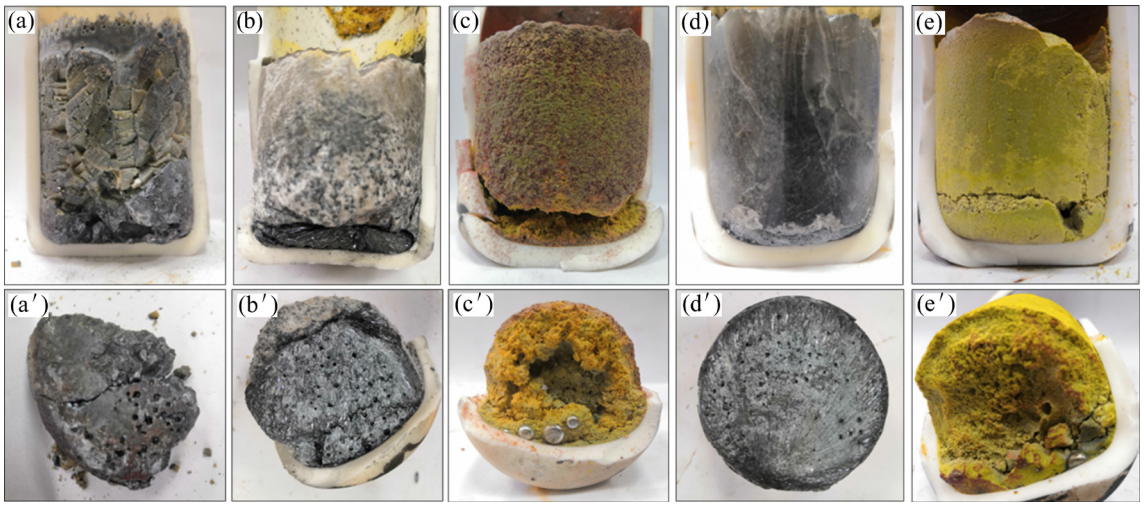


**Fig. 4** Dissolution side view (a−e) and upward view (a′−e′) of $Sb_2S_3$ in different molten salt systems at 850 °C: (a, a′) NK; (b, b′) CN; (c, c′) NN; (d, d′) CNK; (e, e′) NNK

in molten salt physically or chemically to form a uniform phase.

$$4Sb_2S_3+12Na_2CO_3=8Sb+9Na_2S+3Na_2SO_4+9CO_2(g) \quad (1)$$

As shown in Fig. 5, the distribution behavior of $Sb_2S_3$ in the dissolution process was further determined. In the NK system, $Sb_2S_3$ dissolved in the molten salt was low, and its content was only 4%. The volatilization of $Sb_2S_3$ in fume reached 22%, which was the leading cause of raw material loss in the electrolysis process. In the CNK system, the volatilization of $Sb_2S_3$ was effectively reduced to 6%. However, the content of dissolved $Sb_2S_3$ in molten salt was further decreased to 3%. It is not conducive to the improvement of current efficiency. As shown in NN and NNK systems, adding $Na_2CO_3$ can effectively make the solubility of $Sb_2S_3$ in molten salt reach more than 92%, and only about 2% of $Sb_2S_3$ in the fume. Significantly, compared with the NN system, the NNK system has less $Na_2CO_3$ but generates more metal antimony, which may be due to the formation of melt with better fluidity in the ternary system, speeding up the reaction speed of Reaction (1).

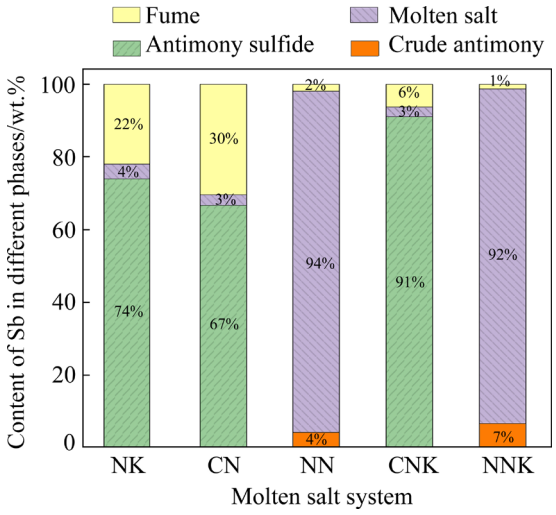


**Fig. 5** Distribution of Sb during $Sb_2S_3$ dissolution in different systems

As shown in Fig. 6, the diffraction pattern of the upper molten salt dissolved by $Sb_2S_3$ showed the NaCl and KCl phases in the NK system. Moreover, no characteristic peak of the dissolved sulfur−antimony compound was found due to its low solubility in the molten salt. In the bottom antimony matte, the main phases were $K(Sb_5S_8)$, KCl, and $NaSbS_2$, and $Sb_2S_3$ was not observed.

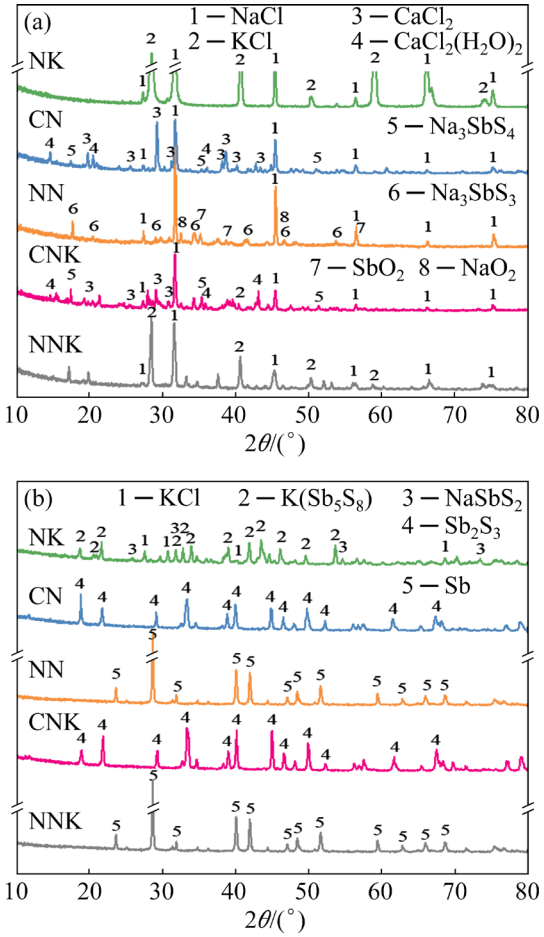


**Fig. 6** XRD patterns of dissolved $Sb_2S_3$ in different systems: (a) Molten salt; (b) Sulfide or crude antimony

Therefore, $Sb_2S_3$ in the system may react with the $Na_2S$ and KCl dissolved in molten salt, which may be a fundamental reason why $Na_2S$ can improve the electrolysis efficiency [18]. In the CN and CNK systems added by $CaCl_2$, there was a soft $Na_3SbS_4$ diffraction peak in the dissolved molten salt, indicating that part of $Sb_2S_3$ is oxidized into the molten salt. According to Reactions (2)−(5), this process may be mainly caused by the release of a large amount of heat when $Na_2S·9H_2O$ was added and contacted with $CaCl_2$, which accelerated the oxidation of $Na_2S$ by air, resulting in the generation of a large amount of $Na_2S_2$. The antimony matte phase was still $Sb_2S_3$ and did not react with the added $Na_2S$ to form $NaSbS_2$. In NN and NNK systems with $Na_2CO_3$ added, $Na_2CO_3$ could not be found in the dissolved molten salt according to the diffraction pattern. Besides NaCl, KCl, $NaSbS_3$, and other halides or sodium thioantimonate, there were diffraction characteristic peaks of $SbO_2$ and $Na_2O$ oxide phases in molten salt. The results show that,

besides the precipitation of crude antimony, some side reactions also occur, making $Sb_2S_3$ have good solubility in the system.

$$4Na_2S+O_2+2H_2O=4NaOH+2Na_2S_2 \quad (2)$$

$$Na_2S+Sb_2S_3=2NaSbS_2 \quad (3)$$

$$2NaSbS_2+Na_2S=2Na_3SbS_3 \quad (4)$$

$$Na_2S_2+Na_3SbS_3=Na_3SbS_4+Na_2S \quad (5)$$

To better understand dissolution characteristics of $Sb_2S_3$ in different systems, SEM−EDS was used to observe the molten salt after its dissolution. As shown in Fig. 7, antimony compounds dissolved in massive form could be found in the binary molten salt systems, NK, CN, and NN. The low content of dissolved Sb and S in molten salt shows that the element Sb primarily existed in the form of small fast sulfide. In the CN system, the particles of thioantimonate are smaller than those of other systems, indicating that the antimony compounds are more difficult to exist stably in molten salt. The content of Sb and S was higher than that of other systems in the NN system. The main distribution areas of Sb and S were overlapped, consistent with the previous analysis results. According to the XRD results, $Na_2CO_3$ was not found, whereas the distribution of O element compatible with part of Na element could be observed. In addition, it is known that the block-soluble antimony compounds play an essential role in the dissolution of $Sb_2S_3$ in molten salts.

Compared with binary molten salt, the ternary system shows advantages in reducing eutectic temperature. The element orientation is also quite different from that of the binary system in $Sb_2S_3$ dissolution. Therefore, to further understand the characteristics of the ternary system, SEM−EDS characterization of CNK and NNK ternary systems were carried out in Fig. 8. The results show that the specific crystal type of the CNK system could not be observed due to the water absorption effect of $CaCl_2$, and NaCl and KCl existing as mosaic crystals. Furthermore, the content of Sb and S in the molten salt was less, and the antimony sulfur compounds observed also existed in smaller aggregates than in the binary system. In the NNK system, it can be found that the regions of Sb and S were overlapped and interlaced with molten salts Na, K, and O.

### 3.4 Constant-voltage electrolysis

#### 3.4.1 Distribution behavior

Constant-voltage electrolysis experiments in different electrolytic systems were carried out under the conditions of temperature 850 °C, cell voltage 2.5 V, electrode spacing 4 cm, electrolytic time 3 h, $Na_2S$ addition 2%, and a material ratio 5:1. The

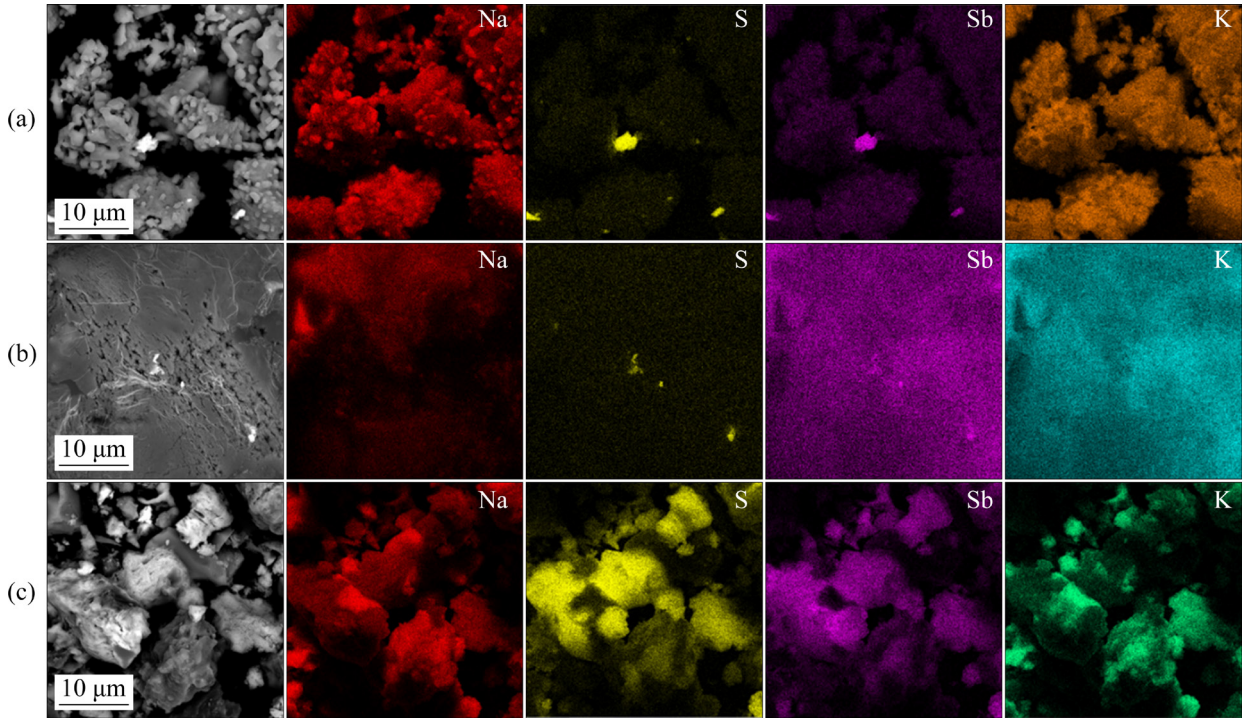


**Fig. 7** SEM−EDS results of $Sb_2S_3$ dissolved in binary systems: (a) NK; (b) CN; (c) NN

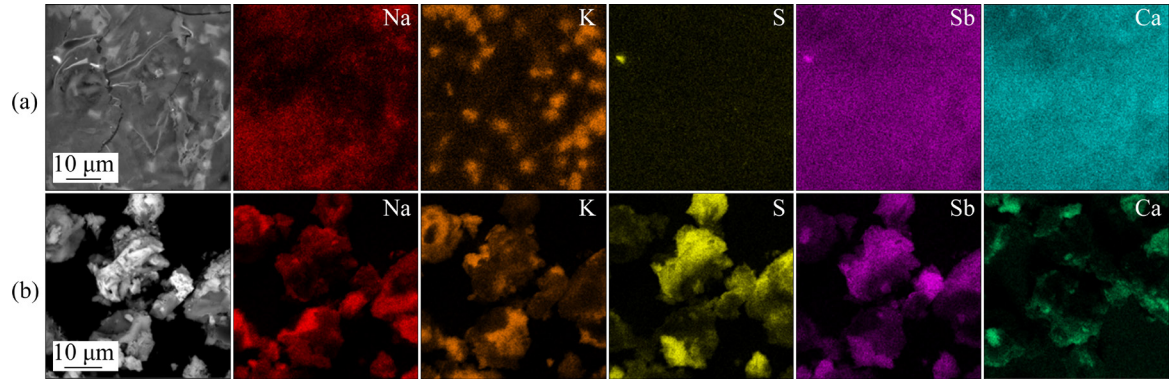


**Fig. 8** SEM−EDS results of $Sb_2S_3$ dissolved in ternary systems: (a) CNK; (b) NNK

cathode (Eq. (6)) and anode (Eq. (7)) reactions can be written as follows [20]. The reaction locations were at the bottom of the anode and the surface of the cathode (antimony liquid).

Cathode reaction:

$$Sb_2S_3(l)+6e=2Sb(l)+3S^{2-} \quad (6)$$

Anode reaction:

$$3S^{2-}=3/xS_x+6e \quad (7)$$

As shown in Fig. 9, the content of metal antimony in NK and NNK systems was more than 50%, indicating that metal antimony has high electrolytic efficiency. 14% of antimony was volatilized into fume in the NK system, limiting the final recovery rate. In the NNK system, the loss of antimony by volatilization of fume only accounted for 2%. However, according to the dissolution test, adding $Na_2CO_3$ could react with part of $Sb_2S_3$ to precipitate metal antimony so that the molten salt had a specific loss. In the NN system, the proportions of antimony in metal antimony and fume were 32% and 5%, respectively. Compared with the ternary NNK system, the proportion of antimony entering metal was lower, and the loss of fume volatilization was higher. In CN and CNK systems, metal antimony accounted for 16% and 18% after electrolysis. Adding $CaCl_2$ is not conducive to improving electrolysis efficiency, probably due to the low solubility of $S^{2-}$ in molten salt by adding $CaCl_2$. It is worth noting that the content of antimony in the fume of the ternary CNK system was only 4%. This proves that adding $CaCl_2$ can effectively limit the evaporation loss of $Sb_2S_3$ in the electrolysis process.

3.4.2 Characterization of molten salt after electrolysis

To further investigate chemical composition of molten salt after electrolysis, the molten salt residue was characterized by XRD. As shown in Fig. 10, the diffraction peaks of NaCl and KCl were observed in the NK system, indicating that the molten salt is stable during electrolysis. Although the electrolyte composition did not change, no residual Sb or S phase was observed. $Na_3SbS_49(H_2O)$ with high chemical valence (+5) was found in the NN and NNK systems residue, which was different from the phase obtained in the dissolution process of $Sb_2S_3$, possibly due to the partial formation of high antimony in electrolysis. Meanwhile, $Na_2CO_3$ was not observed in the diffraction pattern. After electrolysis, the initial molten salt phase could also be found in the CN and CNK systems, indicating the chemical stability of the molten salt system. However, electrolytic residue also has good water absorption. This unfavorable factor probably causes great trouble to the actual industrial production.

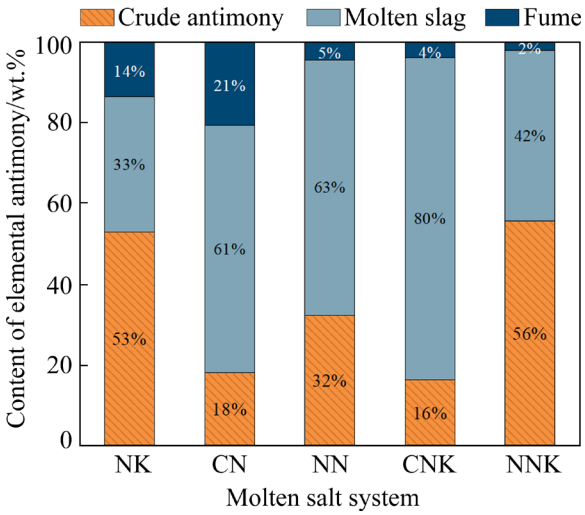


**Fig. 9** Distribution of elemental antimony in crude antimony, molten slag, and fume in different systems

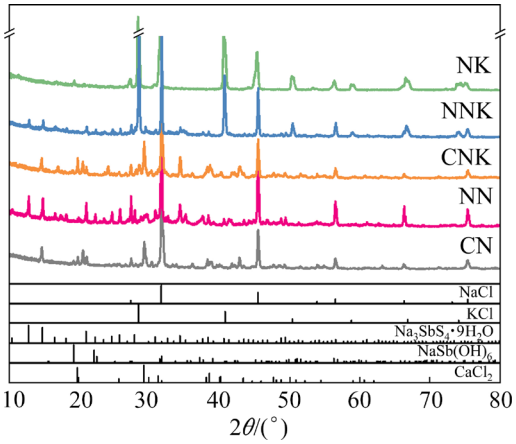


**Fig. 10** XRD patterns of electrolytic residue of molten salt in different systems

### 3.5 Energy consumption calculation

As shown in Fig. 11, current efficiency and energy consumption of the electrolysis process in different systems were investigated. According to Eqs. (8)−(12) [13], the total resistance ($R$), current efficiency ($\eta$), and energy consumption ratio ($R_{EC}$) of each system were calculated:

$$R=U/I \tag{8}$$

$$Q_{\text{theoretical}}=\frac{z\cdot F\cdot m_{\text{Sb}}}{M_{\text{Sb}}} \tag{9}$$

$$Q_{\text{actual}}=I\cdot t \tag{10}$$

$$\eta=\frac{Q_{\text{theoretical}}}{Q_{\text{actual}}}\times 100\% \tag{11}$$

$$R_{\text{EC}}=\frac{U\cdot F\cdot z}{3600M_{\text{Sb}}\cdot\eta} \tag{12}$$

where $U$ is the cell voltage, V; $I$ is the average current, A; $Q_{\text{theoretical}}$ is the theoretical charge quantity, C; $z$ is the number of electron transfer; $F$ is Faraday constant, 96485 C/mol; $m_{\text{Sb}}$ is the mass of antimony, g; $M_{\text{Sb}}$ is the molar mass of Sb, 121.76 g/mol; $t$ is the electrolytic time, s.

In the electrolysis process, except for the NNK system, the current of other systems showed an apparent decreasing trend with time and tended to be stable after 2 h in Fig. 11(a). In the NNK system,

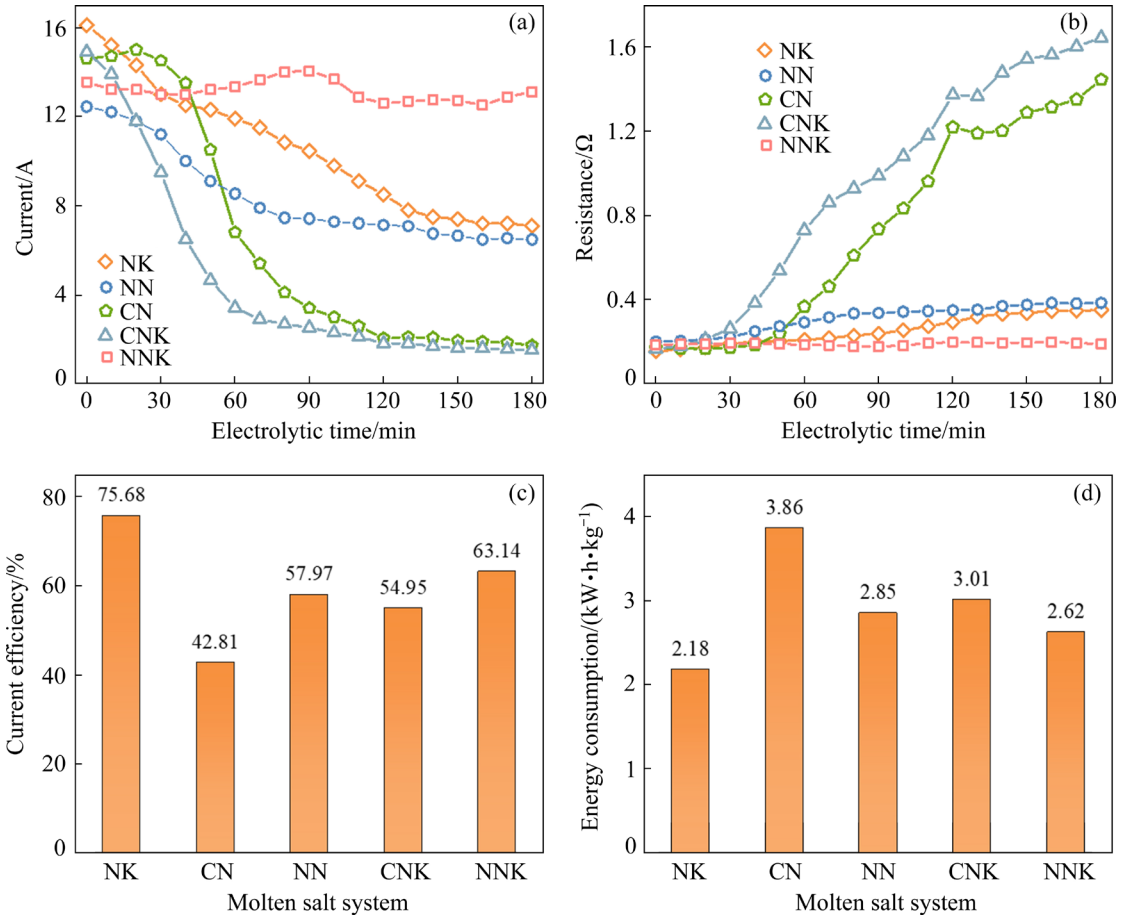


**Fig. 11** Analysis of electrolysis process and electric efficiency in different molten salt systems: (a) Relationship between electrolytic time and current; (b) Relationship between electrolytic time and resistance; (c) Current efficiency after 3 h of electrolysis; (d) Energy consumption after 3 h of electrolysis

the current did not decrease rapidly because of the large amount of dissolved sulfide, which kept the conductivity of the system high. As shown in Fig. 11(b), the resistance of the system at the early electrolysis stage was about 0.2 Ω. With the increase of electrolysis time to 30 min, the resistances of CN and CNK systems increased rapidly, reaching 1.5 and 1.6 Ω, respectively. The resistance of other systems also increased slightly, and the resistance of the whole process was less than 0.4 Ω. This phenomenon resulted from the gradual decrease of $S^{2-}$ or $Sb^{3+}$ concentration near the electrode during electrolysis. In particular, according to previous reports, the solubility of $S^{2-}$ in $CaCl_2$ was minimal, which was a reasonable explanation for the rapid growth of resistance of molten salt by adding $CaCl_2$ [24].

Figures 11(c, d) show the current efficiency and energy consumption of different systems. In the NK system, the current efficiency was the highest at 75.68%, and the energy consumption was only 2.18 kW·h/kg. Compared with the NK system, the NNK system with $Na_2CO_3$ added could effectively improve the direct yield of crude antimony, but the current efficiency was reduced. In CN and CNK systems, the current efficiencies were 42.81% and 54.95%, respectively, and energy consumptions were 3.86 and 3.01 kW·h/kg, respectively. Compared with other systems, it had lower current efficiency but higher energy consumption.

## 4 Conclusions

(1) Selecting a multi-component system may be an effective way to reduce the minimum eutectic temperature of the molten salt system. In addition, adding $Na_2CO_3$ to the molten salt system can increase the solubility and electro-decomposition efficiency of $Sb_2S_3$. The molten salt system added by $CaCl_2$ significantly inhibits the dissolution of $Sb_2S_3$ in the molten salt.

(2) Both NK and NNK systems are beneficial to the electrical decomposition of $Sb_2S_3$, but $Sb_2S_3$ is more likely to volatilize into fume in the NK system. Adding $CaCl_2$ can effectively inhibit the rapid volatilization of $Sb_2S_3$ in molten salt, but it increases the water absorption of molten salt and dramatically reduces the current efficiency.

(3) From the perspective of the energy consumption, NK system has certain advantages, with current efficiency of 75.68% and an energy consumption of only 2.18 kW·h/kg. It is still the more appropriate system for the current investigation. Moreover, the NNK system added by $Na_2CO_3$ is a potential molten salt system, but the appropriate dosage needs further detailed study.

## Acknowledgments

The authors are grateful for the financial supports from the National Natural Science Foundation of China (No. 52074362).

## References

[1] ANDERSON C G. The metallurgy of antimony [J]. Chemie der Erde, 2012, 72: 3−8.

[2] LIANG Y H, LIU Q C, LI Y K, LIU F. Speciation analysis and ecological risk assessment of antimony in Xikuangshan, Hunan Province [J]. Polish Journal of Environmental Studies, 2021, 30(2): 1289−1296.

[3] ZHOU X, ZGAO G H, LI Y Q, CHEN J H, CHEN Y. The flotation process, smelting process and extraction products on jamesonite: A review [J]. Minerals Engineering, 2021, 172: 1−9.

[4] HANSELL C. All manner of antimony [J]. Nature Chemistry, 2015, 7: 88.

[5] WEI J C, GUO X M, MARINOVA D, FAN J. Industrial $SO_2$ pollution and agricultural losses in China: Evidence from heavy air polluters [J]. Journal of Cleaner Production, 2014, 64: 404−413.

[6] YANG J G, TANG C B, CHEN Y M, TANG M T. Separation of antimony from a stibnite concentrate through a low-temperature smelting process to eliminate $SO_2$ emission [J]. Metallurgical and Materials Transactions B, 2011, 42: 30−36.

[7] NAN T X, YANG J G, TANG C B, WANG W C, LONG W, YANG J Y. Hydrometallurgical process for extracting bismuth from by-product of lead smelting based on methanesulfonic acid system [J]. Transactions of Nonferrous Metals Society of China, 2022, 32: 319−332.

[8] AWE S A, SANDSTROM A. Electrowinning of antimony from model sulphide alkaline solutions [J]. Hydrometallurgy, 2013, 137: 60−67.

[9] AWE S A, SUNDKVIST J E, SANDSTROM A. Formation of sulphur oxyanions and their influence on antimony electrowinning from sulphide electrolytes [J]. Minerals Engineering, 2013, 53: 39−47.

[10] SOLOZHENKIN P M, ALEKSEEV A N. Innovative processing and hydrometallurgical treatment methods for complex antimony ores and concentrates. Part II: Hydrometallurgy of complex antimony ores [J]. Journal of Mining Science, 2010, 46(4): 446−452.

[11] TESAROVA E, VYTRAS K. Potentiometric stripping analysis at antimony film electrodes [J]. Electroanalysis, 2009, 21(9): 1075−1080.

[12] WANG X, LIAO C F. Preparation and characterization of tungsten powder through molten salt electrolysis in a

$CaWO_4$−$CaCl_2$−NaCl system [J]. International Journal of Refractory Metals and Hard Materials, 2012, 31: 205−209.
[13] ZHOU Z R, HUA Y X, XU C Y, LI Y, LI X, ZHANG Z. Electrolytic synthesis of ferrotitanium powders from ilmenite in $CaCl_2$−NaCl melts at a lower temperature of 700 °C [J]. Journal of Alloys and Compounds, 2017, 726: 1124−1131.
[14] LU X, ZHANG Z Y, HIRAKI T, TAKEDA O, ZHU H M, MATSUBAE K, NAGASAKA T. A solid-state electrolysis process for upcycling aluminium scrap [J]. Nature, 2022, https://doi.org/10.1038/s41586-022-04748-4.
[15] CHEN G Z, FRAY D J, FARTHING T W. Direct electrochemical reduction of titanium dioxide to titanium in molten calcium chloride [J]. Nature, 2000, 407: 361−364.
[16] RAJPURE K Y, BHOSALE C H. $Sb_2S_3$ semiconductor−septum rechargeable storage cell [J]. Materials Science Communication, 2000, 64: 70−74.
[17] KARTEA L, DARYAL M B, SIRELI G K, TIMUR S. One-step electrochemical reduction of stibnite concentrate in molten borax [J]. International Journal of Minerals, Metallurgy and Materials, 2019, 26(10): 1258−1265.
[18] COLOM F, CRUZ M D L. Antimony electrowinning form molten sulphide [J]. Electrochimica Acta, 1969, 14: 217−221.
[19] TAN M S, HE R, YUAN Y T, WANG Z Y, JIN X B. Electrochemical sulfur removal from chalcopyrite in molten NaCl−KCl [J]. Electrochimica Acta, 2016, 213: 148−154.
[20] YIN H Y, CHUNG B, SADOWAY D R. Electrolysis of a molten semiconductor [J]. Nature Communications, 2016, 7: 12548.
[21] MOHAPATRA O P, ALCOCK C B, JACOB K T. Solubilities of $Pb^{+2}$, $Bi^{+3}$, $Sb^{+3}$, and $Cu^{+1}$ sulfides in (NaCl + KCl + $Na_2S$) melts [J]. Metallurgical Transactions, 1973, 4: 1755−1762.
[22] ZHU Q, YANG J G, TANG C B, NAN T X, DING R Z, LIU J. Electroreduction of antimony sulfide enhanced by nitrogen bottom blowing in molten NaCl−KCl−$Na_2S$ [J]. JOM, 2022, 74(5): 1889−1899.
[23] CHEN Y M, YE L G, TANG C B, YANG S H, TANG M T, ZHANG W H. Solubility of Sb in binary $Na_2CO_3$−NaCl molten salt [J]. Transactions of Nonferrous Metals Society of China, 2015, 25: 3146−3151.
[24] GAO B L, NIU H K, GUAN Y C, WANG Z W, LIU J J, TAYLOR M P, CHEN J J J. Visualization of anode effect in aluminum electrolysis [J]. Journal of the Electrochemical Society, 2022, 169: 013505.

# 不同熔盐体系中 $Sb_2S_3$ 一步电还原脱硫

朱 强，杨建广，唐朝波，丁瑞泽，南天翔，胡晴程

中南大学 冶金与环境学院，长沙 410083

**摘 要：**对 NaCl−KCl、NaCl−$CaCl_2$、NaCl−$Na_2CO_3$、NaCl−KCl−$CaCl_2$ 和 NaCl−KCl−$Na_2CO_3$ 熔盐体系开展比较分析，研究不同熔盐体系的相图、热稳定性和硫化锑的溶解度。根据锑元素分布特征、电流效率、能耗及熔渣成分表征结果，优选出适合 $Sb_2S_3$ 电解还原的熔盐体系。结果表明，所有熔盐体系均具有良好热稳定性，且可实现 $Sb_2S_3$ 的电解还原。添加 $CaCl_2$ 的体系不利于 $Sb_2S_3$ 溶解，而添加 $Na_2CO_3$ 的体系会与 $Sb_2S_3$ 发生反应。此外，NaCl−KCl 体系的电流效率最高(75.68%)，且能耗最低(2.18 kW·h/kg)。

**关键词：**锑冶炼；熔盐电解；$Sb_2S_3$；共晶体系

**(Edited by Bing YANG)**